Eur. Phys. J. B **12**, 555–567 (1999)

THE EUROPEAN PHYSICAL JOURNAL B

EDP Sciences

Diffusion, localization and dispersion relations on "small-world" lattices

R. Monasson[a]

CNRS - Laboratoire de Physique Théorique de l'ENS[b], 24 rue Lhomond, 75231 Paris Cedex 05, France

Received 23 March 1999

Abstract. The spectral properties of the Laplacian operator on "small-world" lattices, that is mixtures of unidimensional chains and random graphs structures are investigated numerically and analytically. A transfer matrix formalism including a self-consistent potential *à la* Edwards is introduced. In the extended region of the spectrum, an effective medium calculation provides the density of states and pseudo relations of dispersion for the eigenmodes in close agreement with the simulations. Localization effects, which are due to connectivity fluctuations of the sites are shown to be quantitatively described by the single defect approximation recently introduced for random graphs.

PACS. 63.50.+x Vibrational states in disordered systems – 71.23.An Theories and models; localized states – 71.55.Jv Disordered structures; amorphous and glassy solids

1 Introduction

Diffusion in random media is an an issue of great practical and theoretical importance which has a received a lot of attention in the past years [1–5]. The presence of disorder, *e.g.* impurities or random site energies, lattice defects, ... may induce the localization of eigenstates and therefore have dramatic consequences on transport properties [2,6–8]. The understanding of the localization transition, based on scaling theory for finite-dimensional systems [9] has also greatly benefited from the study of models on tree-like architecture [10], that is without any underlying geometry. Diffusion on such amorphous structures has also attracted attention as a toy-model of dynamical evolution in the phase space of complex, *e.g.* glassy systems [11,12].

Recently, it was pointed out that mixed lattices, built from a mixture of finite-dimensional structures and random graphs could be of interest to modelize various real situations taking place in different scientific fields [13]. As a main attractive feature, these "small-world" models simultaneously combine short- and long-range interactions and could display some new and interesting properties stemming from this unusual coexistence, see [13–16] and references therein.

From a physical point of view, this situation is already encountered in the field of polymers or more generally long molecules [17]. Couplings between successive monomers give rise to a unidimensional system while (*e.g.* hydrodynamics) interactions between constituents in the three-dimensional space are of long range nature along the polymeric chain. Of course, the long-range links formed this way are strongly correlated and cannot be considered to be independent as in the small-world paradigm. Some successful approximation schemes developed in the context of polymer theory, *e.g.* the self-consistent potential of Edwards [18,19] method precisely amount to neglect such correlations and nevertheless obtain reliable results [17]. Following Zimm's work [20], many studies have concentrated on the influence of such interactions on the relaxation dynamics of polymers [17,21]. However, these calculations can in a sense be considered as *annealed* since the hydrodynamical interactions tensor is averaged over chain positions *before* normal modes are computed and not *later* as it should. Such a pre-averaging approximation [21] may lead to qualitatively erroneous predictions especially for large eigenvalues and must be considered with caution. Diffusion on the small-world lattice can therefore be viewed as an elementary step toward the understanding of small times vibrations or equivalently the instantaneous normal modes [22–24] of a polymeric chain around a *quenched* configuration.

From a theoretical point of view, the small-world structure is also worth being investigated since it mixes two structures which can be studied in great mathematical details [13]. Diffusion on a one-dimensional lattice obviously reduces to the study of dispersion relations for plane waves [3]. As for the random graph structure, a large attention has also been paid to its spectral properties [12,25–29]. The main physical feature is the emergence of localized states centered on the geometrical defects of the graph, that is sites with abnormally low

[a] e-mail: monasson@physique.ens.fr

[b] LPTENS is a unité mixte du CNRS, associée à l'École Normale Supérieure et à l'Université de Paris–Sud.

or large connectivities with respect to the average coordination number [27]. As we shall see, the combination of both structures can be precisely studied and allows to answer some interesting questions concerning localization and the existence of pseudo-dispersion relations for the eigenmodes in presence of disorder [8,30].

This paper is organized as follows. In Section 2, the small-world model is defined and related to its building bricks, that is a random graph superposed to a one-dimensional lattice. The main features of diffusion on the latters are briefly recalled and used to guess some spectral properties of the small-world Laplacian. Section 3 exposes the numerical results obtained from exact diagonalizations. The density of states as well as some characteristics of the eigenmodes, *e.g.* localization properties and autocorrelation functions are analyzed. We present in Section 4 the analytical approach to attack the problem, based on a self-consistent transfer matrix formalism [18,19]. The region of the spectrum corresponding to extended eigenstates is studied in Section 5 by means of an effective medium approximation [1,30]. Localization properties are unravelled in Section 6 using a more refined scheme of approximation exploiting the geometrical defect mechanism exposed above [27].

2 The small-world lattice and its structure

2.1 Presentation of the model

We consider N points A_i, $i = 1, \ldots, N$ on a one-dimensional ring $\mathcal{R}$. Each point A_i is connected to its $2K$ nearest neighbors $A_{i\pm1}, A_{i\pm2}, \ldots, A_{i\pm K}$ (where site labels are defined modulo N to ensure periodicity on $\mathcal{R}$). In addition, we superpose to $\mathcal{R}$ a random graph $\mathcal{G}$ with mean connectivity q defined as follows. Each pair of points (A_i, A_j) (such that the distance $|i-j|$ on the ring is larger than K) is connected with probability q/N and left unchanged with probability $1 - q/N$.

The small-world lattice $\mathcal{S}$ is the union of both graphs $\mathcal{R}$ and $\mathcal{G}$. In average, $\mathcal{S}$ includes $(K + q/2)N$ edges to largest order in N. The coordination degree c_i of A_i is a random variable bounded from below by $2K$. More precisely, $c_i - 2K$ obeys a Poisson law of parameter q. This "small-world" lattice differs from the definition of [13] but maintains the coexistence between short- and long-range links. In addition it leads to simpler analytical calculations than the model exposed in [13].

Then we consider the Laplacian operator $W^{\mathcal{S}}_{ij}$ on $\mathcal{S}$. For $i \neq j$, $W^{\mathcal{S}}_{ij} = -1/2K$ if A_i and A_j are connected, 0 otherwise. Diagonal elements, $W^{\mathcal{S}}_{ii} = c_i/2K$ ensure the conservation of probability. Note that, with respect to the usual definition, eigenvalues are rescaled by a multiplicative factor $-1/2K$ so that the support of the spectrum becomes positive.

2.2 Definition of spectral quantities

We call λ_e (respectively $w_{j,e}$) the eigenvalues (respectively the components of the associated eigenvectors normalized to unity) of the Laplacian $W^{\mathcal{S}}$, with $e = 1, \ldots, N$. Most spectral properties of $W^{\mathcal{S}}$ can be obtained through the calculation of the resolvent [7]

$$G^{\mathcal{S}}_{jk}(\lambda + \mathrm{i}\epsilon) = \left((\lambda + \mathrm{i}\epsilon) 1 - W^{\mathcal{S}} \right)^{-1}_{jk} = \sum_{e=1}^{N} \frac{w_{j,e} w_{k,e}}{\lambda - \lambda_e + \mathrm{i}\epsilon} \cdot \tag{1}$$

The mean density of eigenvalues indeed reads

$$p(\lambda) = -\frac{1}{N\pi} \lim_{\epsilon \to 0^+} \sum_{j=1}^{N} \mathrm{Im}\, \overline{G^{\mathcal{S}}_{jj}(\lambda + \mathrm{i}\epsilon)}, \tag{2}$$

where the overbar denotes the average over disorder, that is the random graph $\mathcal{G}$.

Another quantity of interest is the autocorrelation function of eigenvectors. The power spectrum $|\tilde{w}_e(\theta)|^2$ of eigenmode e, *i.e.* the squared modulus of its Fourier transform reads

$$|\tilde{w}_e(\theta)|^2 = \sum_{j,k=1}^{N} w_{j,e} w_{k,e} \exp(2\mathrm{i}\pi\theta(j-k)). \tag{3}$$

Then we define $|\tilde{w}(\theta, \lambda)|^2$ as the sum of $|\tilde{w}_e(\theta)|^2$ over all $w_{i,e}$ lying in the range $\lambda \leq \lambda_e \leq \lambda + \mathrm{d}\lambda$, divided by the number $Np(\lambda)\mathrm{d}\lambda$ of such eigenvectors. Once ensemble average is carried out, this power spectrum is simply related to the off-diagonal resolvent (1) through

$$\frac{1}{N} \sum_{j,k=1}^{N} \overline{G^{\mathcal{S}}_{jk}(\lambda + \mathrm{i}\epsilon)} \exp(2\mathrm{i}\pi\theta(j-k)) = \int_0^\infty \mathrm{d}\mu\; p(\mu)\; \frac{\overline{|\tilde{w}(\theta,\mu)|^2}}{\lambda - \mu + \mathrm{i}\epsilon}, \tag{4}$$

where we have assumed that the density of states p is self-averaging [31], as confirmed by numerics when the size of the sample N becomes large.

Localization properties of eigenmodes can be studied through the knowledge of inverse participation ratios [2,7]. The inverse participation ratios of eigenmodes e, defined as $w^4_e = \sum_i |w^{(e)}_i|^4$ are then averaged over a small energy region around λ to give $w^4(\lambda)$ following the procedure described above. Though inverse participation ratios may fluctuate from state to state at a given eigenvalue λ, a non vanishing value of the ensemble averaged $\overline{w^4(\lambda)}$ gives a good indication of the emergence of localization [2].

The spectral properties of $\mathcal{S}$ will of course reflect its mixed structure. Before turning to numerics, it is therefore useful to briefly recall known results on the spectral properties of both $\mathcal{R}$ and $\mathcal{G}$ separately.

2.3 Diffusion on the unidimensional ring

On the ring, the Laplacian operator $W^{\mathcal{R}}$ is diagonalized by plane waves w_ϕ whose components at site j read

$$(w_\phi)_j = \frac{1}{\sqrt{N}} \exp(2\mathrm{i}\pi\phi j), \tag{5}$$

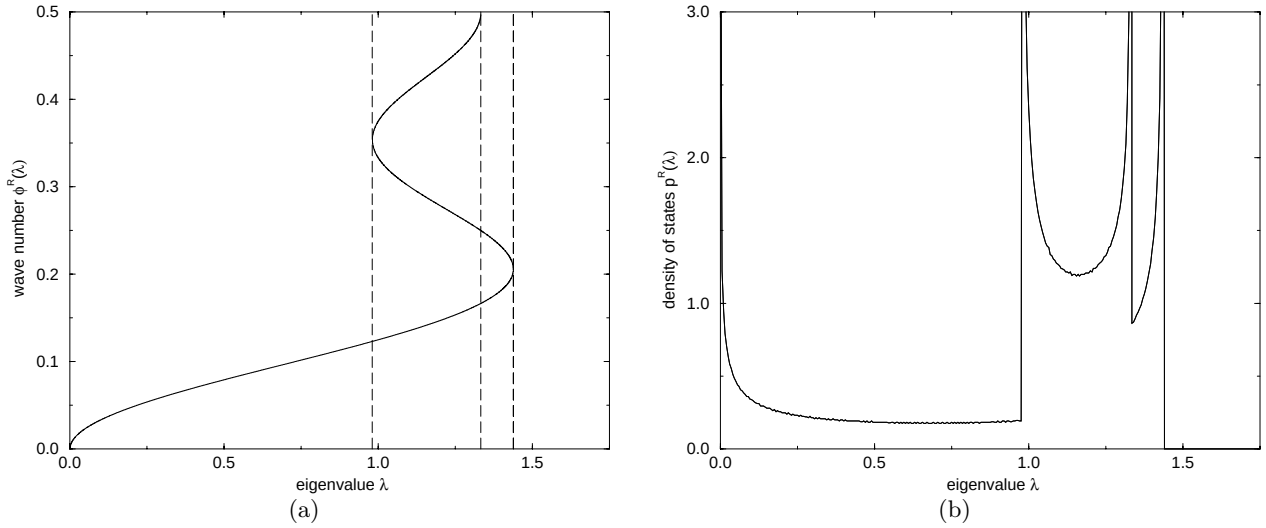

Fig. 1. The $K = 3$ ring. (a) Relation of dispersion; the plane wave phase $\phi^{\mathcal{R}}(\lambda)$ is plotted as a function of the eigenvalue λ(full curve). Non zero stationary eigenvalues are indicated by dashed lines (from left to right: $\lambda_2^{\mathcal{R}}$, $\lambda_3^{\mathcal{R}}$ and $\lambda_1^{\mathcal{R}}$, see text). (b) Density of states $p^{\mathcal{R}}(\lambda)$ as a function of λ. Van Hove singularities take place at $\lambda_0^{\mathcal{R}}$, $\lambda_2^{\mathcal{R}}$, $\lambda_3^{\mathcal{R}}$ and $\lambda_1^{\mathcal{R}}$ (from left to right)

where the phase ϕ assumes multiple values of $1/N$, from 0 up to $1-1/N$. In the large N limit, ϕ becomes a continuous variable ranging from $0 \leq \phi < 1$ and the corresponding eigenvalue is given by

$$\lambda^{\mathcal{R}}(\phi) = 1 - \frac{1}{K}\sum_{\ell=1}^{K} \cos(2\pi\ \ell\ \phi). \tag{6}$$

Due to the reflection symmetry $\phi \to 1-\phi$, we can restrict to ϕ belonging to the interval $[0; 1/2]$. The dispersion relation (6) defines the inverse multivalued function $\phi^{\mathcal{R}}(\lambda)$ plotted Figure 1a for $K = 3$. The eigenvalue λ is stationary for four different wave numbers $\phi_0^{\mathcal{R}} = 0$, $\phi_1^{\mathcal{R}} \simeq 0.206$, $\phi_2^{\mathcal{R}} \simeq 0.354$ and $\phi_3^{\mathcal{R}} = 1/2$ corresponding to $\lambda_0^{\mathcal{R}} = 0$, $\lambda_1^{\mathcal{R}} \simeq 1.439$, $\lambda_2^{\mathcal{R}} \simeq 0.981$ and $\lambda_3^{\mathcal{R}} = 4/3$. The density of states $p^{\mathcal{R}}(\lambda)$ is given by

$$p^{\mathcal{R}}(\lambda) = \sum_{\phi/\phi^{\mathcal{R}}(\lambda)=\phi} \frac{1}{|\lambda^{\mathcal{R}}(\phi)'|}, \tag{7}$$

and is shown Figure 1b for $K = 3$. Van Hove singularities are located at $\lambda_0^{\mathcal{R}}$, $\lambda_1^{\mathcal{R}}$, $\lambda_2^{\mathcal{R}}$ and $\lambda_3^{\mathcal{R}}$.

The relation of dispersion may be found back by looking at the autocorrelation function of eigenvectors, or alternatively at their power spectrum $|\tilde{w}(\theta,\lambda)|^2$, see Section 2.2. According to Figure 1a, $|\tilde{w}(\theta,\lambda)|^2$ will exhibit one (respectively two or three) Dirac peaks over the range $0 \leq \theta \leq \frac{1}{2}$ when $0 < \lambda < \lambda_2^{\mathcal{R}}$ (respectively $\lambda_3^{\mathcal{R}} < \lambda < \lambda_1^{\mathcal{R}}$ or $\lambda_2^{\mathcal{R}} < \lambda < \lambda_3^{\mathcal{R}}$). The locations of the peaks coincide with the multivalued function $\phi^{\mathcal{R}}(\lambda)$, giving back the relation of dispersion (6). The study of the power spectrum will turn out to be useful for establishing pseudo-dispersion relations on the small-world lattice in presence of disorder.

2.4 Diffusion on the random graph

Diffusion on the random graph has been the object of several analytical and/or numerical studies [12,25–29]. Briefly speaking, the two main physical features are:

- The spectral density has a bell-like shape with small oscillating tails (see Fig. 1 in [27]). The central bell-like part corresponds to extended states.
- The lateral oscillations are accompanied by increase of the inverse participation ratio, which is an indication of the localization of eigenmodes near mobility edges. Localized states are centered on geometrical defects, that is sites with abnormally large or low connectivities with respect to the average coordination number.

More quantitatively, defects will pin localized states if their connectivity c deviate from the average coordination number q by more than $\pm\sqrt{q}$. Due to the defect mechanism, the localized peak associated to connectivity c has a total weight (*i.e.* integrated density of states) well approximated by the Poisson law $p^c \mathrm{e}^{-p}/c!$

2.5 Perturbation theory and heuristic arguments

We start by decomposing $W^{\mathcal{S}}$ into $W^{\mathcal{R}} + W^{\mathcal{G}}$. One is tempted to treat $W^{\mathcal{G}}$ as a small perturbation with respect to the ring Laplacian $W^{\mathcal{R}}$ when $q \ll 1$. The resolvents $G^{\mathcal{S}}$ and $G^{\mathcal{R}}$ for the small-world lattice and the ring obey the Dyson equation

$$G^{\mathcal{S}}_{jk}(\lambda+\mathrm{i}\epsilon) = G^{\mathcal{R}}_{jk}(\lambda+\mathrm{i}\epsilon) + \sum_{\ell,m=1}^{N} G^{\mathcal{R}}_{j\ell}(\lambda+\mathrm{i}\epsilon) W^{\mathcal{G}}_{\ell m} G^{\mathcal{S}}_{mk}(\lambda+\mathrm{i}\epsilon). \tag{8}$$

Using the above equation, the Fourier transform $\Sigma(\lambda + \mathrm{i}\epsilon, \phi)$ of the averaged self-energy

$$\Sigma_{jk}(\lambda + \mathrm{i}\epsilon) = \left[\overline{G^{\mathcal{R}}(\lambda + \mathrm{i}\epsilon)}\right]^{-1}_{jk} - \left[\overline{G^{\mathcal{S}}(\lambda + \mathrm{i}\epsilon)}\right]^{-1}_{jk}, \quad (9)$$

can be computed order by order within perturbation theory [7].

At first order, the self-energy reads using (5),

$$\Sigma_1(\lambda + \mathrm{i}\epsilon, \phi) = \sum_{j,k=1}^{N} \overline{W^{\mathcal{G}}_{jk}}\ (w_\phi)_j\ (w_\phi)^*_k = \frac{q}{2K}, \quad (10)$$

for non zero phases ϕ. In other terms, the whole spectrum in Figure 1b would be shifted to the right by $q/2K$.

Second order corrections to the self-energy are diagonal in the direct space (when $N \to \infty$) and may be written in the Fourier space as

$$\begin{aligned}\Sigma_2(\lambda+\mathrm{i}\epsilon, \phi) &= \sum_{j,k=1}^{N} \sum_{\ell,m=1}^{N} \overline{W^{\mathcal{G}}_{jk} W^{\mathcal{G}}_{\ell m}}^{\,c} G^{\mathcal{R}}_{k\ell}(\lambda + \mathrm{i}\epsilon)(w_\phi)_j (w_\phi)^*_m \\ &= \frac{q}{2K^2} \int_0^\infty \mathrm{d}\mu\ \frac{p^{\mathcal{R}}(\mu)}{\lambda - \mu + \mathrm{i}\epsilon}, \end{aligned} \quad (11)$$

where the subscript c indicates the connected two-points correlation function of $W^{\mathcal{G}}$. The emergence of an imaginary part in the self-energy shows that the resolvent $\overline{G^{\mathcal{S}}_{jk}}$ at energy level λ will decrease exponentially with the distance $|j-k|$ over a typical length

$$L_E(\lambda) = \frac{2K^2}{\pi}\ q^{-1}\ \left(p^{\mathcal{R}}(\lambda)\right)^{-1}. \quad (12)$$

The latter may be interpreted as the elastic mean path [2,32] travelled by a wave at energy level λ between two successive scattering events. In other words, the peaks appearing in the power spectrum of the eigenvectors (3) will acquire some finite width $\sim 1/L_E$, see Section 4.4. $L_E(\lambda)$ indeed diverges for weak disorder $q \to 0$. Clearly, perturbation theory is sensible as long as the wave length $1/\phi^{\mathcal{R}}(\lambda)$ keeps much smaller than the elastic mean path $L_E(\lambda)$, the so-called Ioffe-Regel criterion [2]. This condition obviously breaks down at van Hove singularities, see Section 2.3. Furthermore, at moderately large eigenvalues ($\lambda > \lambda_2^{\mathcal{R}}$ in the $K = 3$ case), the existence of several distinct branches in the dispersion relation (Fig. 1a) makes the density of states higher than at smaller eigenvalues ($\lambda < \lambda_2^{\mathcal{R}}$) as seen Figure 1b. We therefore expect from expression (12) that disorder will affect the density of states at large eigenvalues more strongly than at small energy levels.

This reasoning should hold except at vanishing eigenvalues λ. One-dimensional model indeed present the peculiarity that the density of states diverges at zero energy. More precisely, $L_E(\lambda) \sim \sqrt{\lambda}$ as $\lambda \to 0$ and therefore perturbation theory should not be trust below $\lambda = O(q)$.

What happens at smaller energy levels? Some heuristic arguments were developed in [12] to answer this equation in the random graph case. First of all, calculations of the spectrum on a Cayley tree with *fixed* connectivity c show a gap between the null eigenvalue and the left side of the spectrum support which disappear in the limit $c \to 2$ only. Indeed, long enough chain-like structure are capable of exhibiting small eigenvalues of the order of their inverse squared length [12]. It is appealing but speculative to think that the small eigenvalues of $W^{\mathcal{S}}$ come from rare portions of the 1-D ring unaltered by disorder [12]. This Lifshitz-like argument may be quantified as follows. A chain of M sites, giving rise to eigenvalues of the order of $1/M^2$ will not be corrupted by the random graph component $\mathcal{G}$ with an exponentially small probability scaling as $\exp(-qM)$. Summing these contributions to the density of states over large M values, we obtain

$$p(\lambda) \simeq p^{\mathcal{R}}(\lambda)\ \exp\left(-\frac{q}{\phi^{\mathcal{R}}(\lambda)}\right), \quad (13)$$

for small λ's. Expression (13) has a nice interpretation in terms of the disordered-induced length $L_d = 1/q$. The eigenmodes of the ring are exponentially attenuated with the ratio of their wave-length over the typical distance L_d between two successive random links incoming onto the one-dimensional structure. When $\lambda \to 0$, the exponential term in (13) vanishes as $\exp(-Cq/\sqrt{\lambda})$ (where C is a constant) and thus screens the algebric divergence of $p^{\mathcal{R}}$. This argument predicts a cross-over between the pure case and the Lifshitz tail at $\lambda_{\mathrm{c.o.}} = O(q^2)$ corresponding to a density $p_{\mathrm{c.o.}} = O(q^{-1})$. We shall see in next sections that such a cross-over is indeed present.

3 Numerical diagonalization

In this section we restrict to $K = 3$. The corresponding ring has a non trivial relation of dispersion giving rise to richer features than for smaller values of the connectivity, *e.g.* $K = 1$. In addition, diagonalizations of small-world lattices with larger K suffer from bigger finite-size effects and thus reliable results demand a prohibitive computing cost.

3.1 Description of the eigenvalues spectrum

We have performed exact numerical diagonalizations of the random Laplacian $W^{\mathcal{S}}$ in the case $K = 3$ for different sizes, up to $N = 1000$ and for 1000 samples. Figures 2a and 2b respectively display $p(\lambda)$ and $w^4(\lambda)$ for connectivity parameters $K = 3, q = 1$. Main remarks are in order:

- The density of states at small eigenvalues seems to vanish for $\lambda < \lambda_- \simeq 0.045 \pm 0.005$. There is no true gap strictly speaking but rather a very small density of states (discussed in Sect. 2.5) that cannot be accounted for by numerics due to the statistical shortfall of eigenvalues. In the following, the $[0; \lambda_-]$ range will be referred to as a "pseudo-gap".
- The density of states exhibit a maximum on the left side of the spectrum at $\lambda_{\mathrm{c.o.}} \simeq 0.11$, slightly above λ_-.

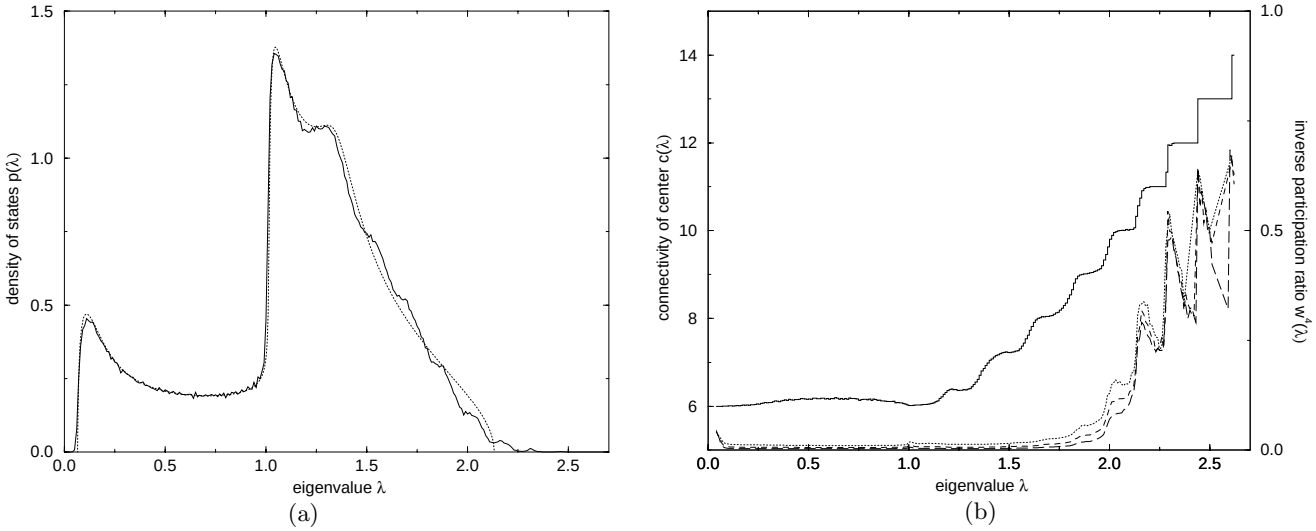

Fig. 2. Results for connectivity parameters $K = 3$, $q = 1$. (a) Density of states p obtained from numerics (full curve) and EMA (dotted line) approximation. (b) Coordination of eigenstate-center c (full curve) and inverse participation ratio w^4 for $N = 256$ (dotted curve), $N = 512$ (dashed curve) and $N = 1000$ (dot-dashed curve) averaged over 1000 samples.

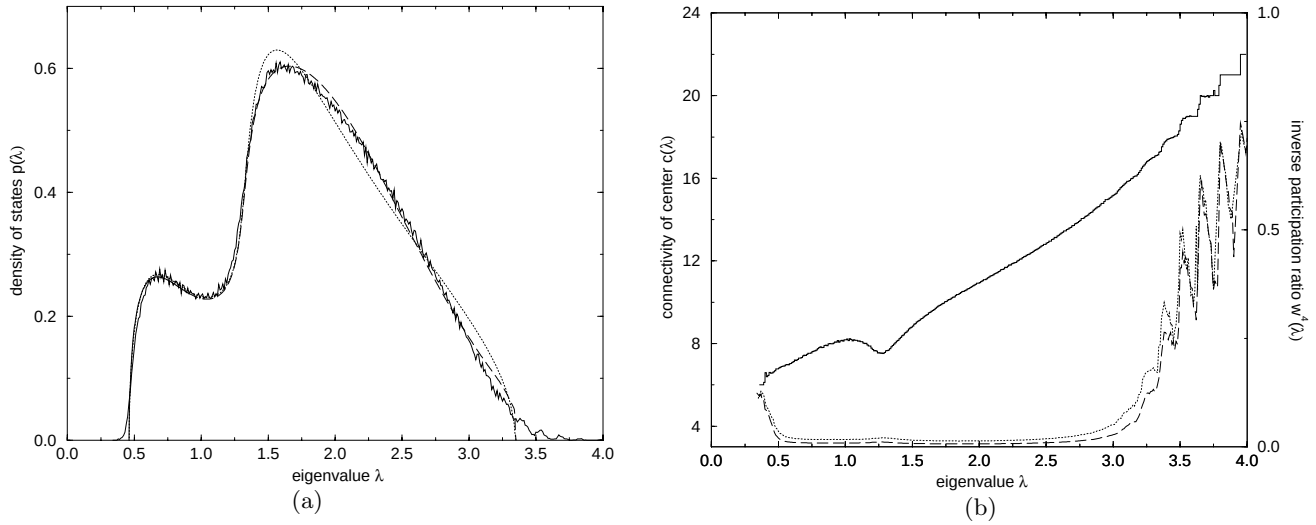

Fig. 3. Results for connectivity parameters $K = 3$, $q = 5$. (a) Density of states p obtained from numerics (full curve), EMA (dotted line) and SDA (dashed line) approximation. (b) Inverse participation ratio w^4 (full curve) and center coordination c for $N = 256$ (dotted curve) and $N = 512$ (dashed curve) averaged over 1000 samples.

– The central part of the spectrum ($\lambda_{\text{c.o.}} < \lambda < \lambda_+$) has a smooth shape and corresponds to extended states. The general form of $p(\lambda)$ is reminiscent of the density of states for the ring Figure 1b but divergences have been smeared out by disorder [8]. Notice that in the range $\lambda_{\text{c.o.}} < \lambda < 1$, the density of states is in quantitative agreement with the ring spectrum, compare Figures 1b and 2a. For increasing sizes N and at fixed λ, w^4 vanishes as $1/N$ and the breakdown of this scaling identifies the upper mobility edge: $\lambda_+ \simeq 2.1 \pm 0.1$.
– On the right side of the spectrum, the density exhibits successive regular peaks and the eigenstates become localized, see Figure 2b.

Similar results are shown Figures 3a and 3b for $K = 3$ and a larger random graph component $q = 5$. In this case, we have found $\lambda_- \simeq 0.4 \pm 0.05$, $\lambda_{\text{c.o.}} \simeq 0.7 \pm 0.05$ and $\lambda_+ \simeq 3.3 \pm 0.1$. As expected, localization effects are stronger and the pseudo-gap becomes wider.

3.2 Relations of dispersion for extended states

Following Section 2.2, we have computed the power spectra $\overline{|\tilde{w}(\theta, \lambda)|^2}$ for different values of λ and connectivity parameters $K = 3, q = 1$ and $K = 3, q = 5$, see Figures 4 and 5 respectively.

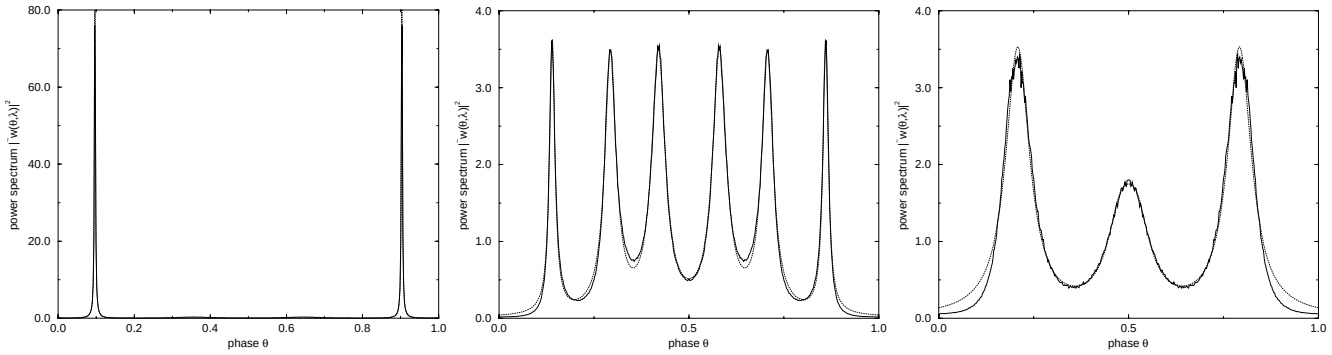

Fig. 4. Power spectrum $\overline{|\tilde{w}(\theta,\lambda)|^2}$ of the eigenvectors as a function of the phase θ for $K=3$, $q=1$ at different energy levels. The dotted lines correspond to the Lorentzian fit (14) of Section 3.2. (a) $\lambda=0.8$. (b) $\lambda=1.2$. (c) $\lambda=1.8$.

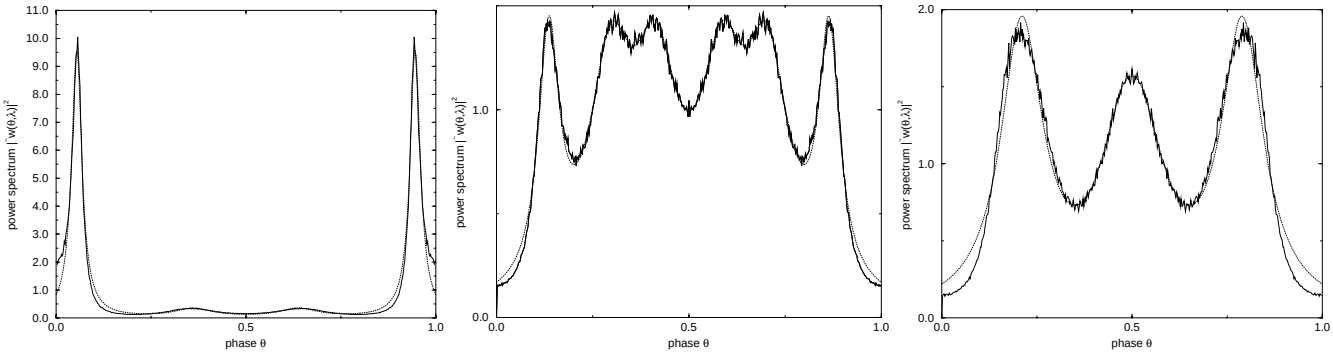

Fig. 5. Same as Figure 4 but with connectivity parameters $K=3$, $q=5$. (a) $\lambda=0.9$. (b) $\lambda=1.7$. (c) $\lambda=2.5$.

Depending on the eigenvalue λ, the power spectrum is mainly composed of different peaks whose number varies from two to six as in the ring case, see Figure 1a. However, these peaks have now non-zero widths, equal to the inverse autocorrelation lengths of the eigenvectors. A good fit on the range $0 \leq \theta \leq 1$ consists in a superposition of 2 m Lorentzian spectra, see Figures 4 and 5,

$$\overline{|\tilde{w}(\theta,\lambda)|^2} \simeq \sum_{\ell=1}^{m} \left[\frac{\tilde{w}_\ell}{4\pi^2(\theta-\phi_\ell)^2+\sigma_\ell^2} + \frac{\tilde{w}_\ell}{4\pi^2(1-\theta-\phi_\ell)^2+\sigma_\ell^2} \right]. \tag{14}$$

Peaks are labelled so that $0 \leq \phi_1 < \ldots < \phi_m$. Close to the pseudo-gap edge λ_-, m equals two and the weight $\tilde{w}_2$ of the secondary peak gets much smaller than $\tilde{w}_1$, see Figures 4a and 5a. As a result, the estimates for ϕ_2, σ_2 becomes less accurate. Moreover, for large eigenvalues, the Lorentzian form (14) does not fit numerical data two well. Consequently, the error bars on ϕ_ℓ, σ_ℓ increase when λ reaches λ_+. We have plotted Figures 6 and 7 the wave numbers ϕ_ℓ and the widths σ_ℓ obtained from the numerical data *vs.* the eigenvalue λ for $q=1$ and $q=5$ respectively.

At first sight, the wave numbers ϕ_ℓ are much less affected by disorder than the overall features of the density of states, *e.g.* the edges λ_- and λ_+ and of course the inverse lengths σ_ℓ (that are equal to zero in the ring case). Indeed, the stationary points in the wave numbers curves Figures 6a and 7a, that is the merging points between ϕ_1, ϕ_2 and ϕ_2, ϕ_3 precisely coincide with the ring values $\phi_1^{\mathcal{R}}$ and $\phi_2^{\mathcal{R}}$ of Section 2.3. The main qualitative difference between the above figures and Figure 1a lies in the appearance of a narrow area surrounded by the ϕ_2 and ϕ_3 lines, centered around $\phi_2^{\mathcal{R}}$ and extending down to $\lambda=\lambda_-$. Thus, contrary to the ring case, the power spectrum of these eigenstates displays more than one peak (even if the heights of the secondary peaks are small as mentioned above).

When λ lies in the range $\lambda_{\text{c.o.}} < \lambda < 1$, σ_1 gets very small, see Figures 6b and 7b. In presence of the disorder, these eigenmodes have conserved an overall quasi-plane wave form. Such a behaviour is indeed expected from Section 2.5. This result explains the quantitative agreement between the density of states of the ring and the numerical spectrum for the small-world lattice observed in Section 3.1 in the intermediate range $\lambda_{\text{c.o.}} < \lambda < 1$.

To end with, let us stress that formula (14) allows us to define some pseudo relations of dispersion characterizing the gross form of eigenmodes at energy λ through some wave numbers ϕ_ℓ and inverse autocorrelation lengths σ_ℓ.

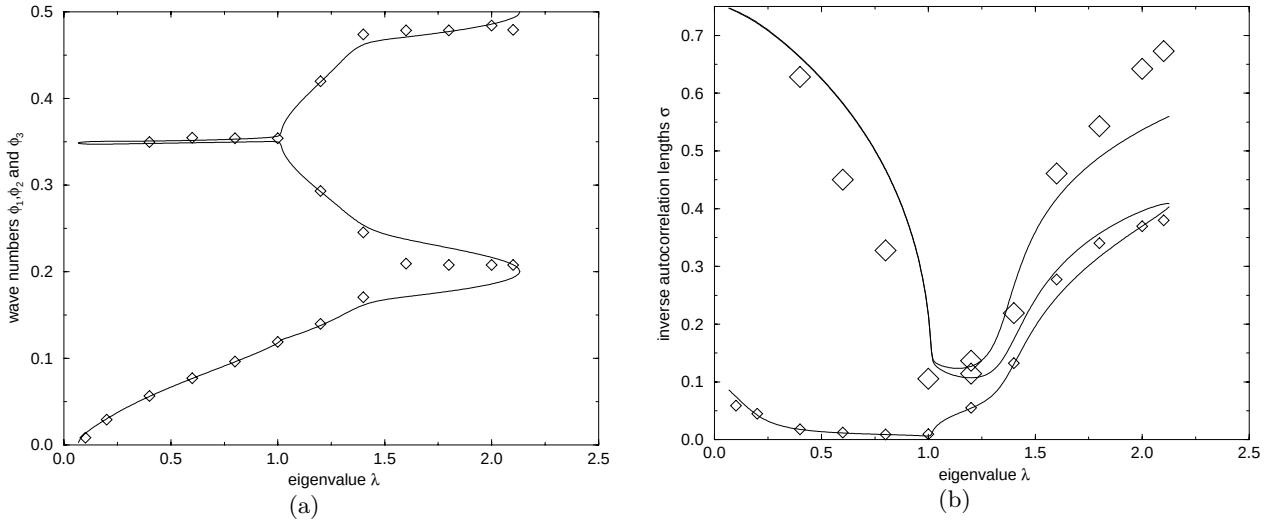

Fig. 6. Effective relation of dispersions for $K = 3$, $q = 1$ obtained from numerical data (squares) and EMA approximation (full line). Error bars correspond to the size of the squares. (a) Wave numbers ϕ_i, (b) inverse autocorrelation lengths σ_i.

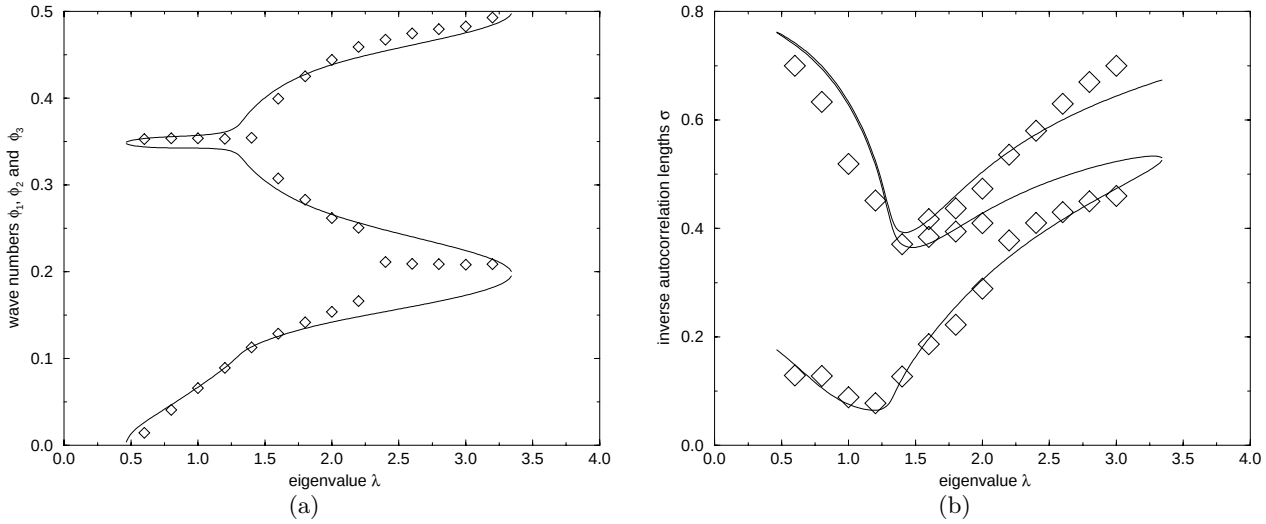

Fig. 7. Same as Figure 6 but with connectivity parameters $K = 3$, $q = 5$.

3.3 Localized eigenstates

Following Section 2.4, we have measured for each eigenvector w_i the connectivity c_ℓ of its center, that is the site i_0 with maximum component $|w_{i_0,e}|$ [27]. The mean connectivity $c(\lambda)$ of the centers of eigenvectors having eigenvalue λ is plotted Figure 2b. It is a smooth monotonous function of λ in the central part of the spectrum. In the localized region, $c(\lambda)$ is constant over a given peak and integer-valued (for $c \geq c_+ = 10$ on the right side); the center connectivity abruptly jumps when λ crosses the borders between peaks.

Tables 1 and 2 list the weights $p_c^{\rm NUM}$ of the localized peaks related to connectivities c, that is the integrated densities of eigenvalues belonging to them. The corresponding eigenvalues $\lambda_c^{\rm NUM}$ are also given. They are measured at the top of the peaks with absolute error ± 0.005 whereas the relative error on $p_c^{\rm NUM}$ is about 20%. The reliability of numerical results suffers from two effects. First, as λ decreases, localized peaks get closer and closer to the flank of the extended spectrum and the determination of the top of the peaks $\lambda_c^{\rm NUM}$ becomes less and less accurate. Secondly, for large eigenvalues, the corresponding statistical events are rare and fluctuate drastically from sample to sample leading to a poor accuracy on $p_c^{\rm NUM}$. Note however that $p_c^{\rm NUM}$ is of the same order of magnitude (but smaller as it should be due to the screening effect exposed in [27]) as the fraction of sites having $c = 2K + c'$ neighbors, with c' given by a Poisson law of parameter q.

Contrary to the random graph case [27], localized peaks are not found on the left side of the spectrum.

Table 1. Case $K = 3, q = 1$: Weights p (*i.e.* integrated density of eigenvalues belonging) of the localized peaks (divided by the Poisson factor $\mathrm{e}^{-q}q^{c'}/c'!$ with $c' = c - 2K$) and corresponding eigenvalues λ for defect connectivities c. Results are obtained from numerical simulations (NUM) and SDA. The accuracy of numerical values is discussed in Section 3.3.

c	11	12	13	14
λ^{NUM}	2.175	2.315	2.460	2.615
λ^{SDA}	2.195	2.325	2.469	2.619
p^{NUM}	0.60	0.78	0.90	0.44
p^{SDA}	0.550	0.686	0.755	0.798

Table 2. Same as Table 1 but with connectivity parameters $K = 3$, $q = 5$.

c	18	19	20	21	22
λ^{NUM}	3.425	3.545	3.685	3.850	3.990
λ^{SDA}	3.433	3.556	3.696	3.841	3.990
p^{NUM}	0.60	0.62	0.79	0.77	0.60
p^{SDA}	0.574	0.696	0.762	0.802	0.831

Indeed, the minimal connectivity of a site in the small-world case is $c = 2K$ and defects with low connectivities with respect to the average coordination $2K + q$ can be seen at very strong disorder only.

4 Theoretical framework

4.1 The average over the disorder

Once averaged over the disorder, the resolvent (1) can be written as the propagator of a replicated Gaussian field theory [7]

$$\overline{G^{\mathcal{S}}_{jk}(\lambda+\mathrm{i}\epsilon)} = \lim_{n\to 0} -\frac{\mathrm{i}}{n}\int\prod_i \mathrm{d}\mathbf{x}_i(\mathbf{x}_j\cdot\mathbf{x}_k) \times\overline{\exp\left(\frac{\mathrm{i}}{2}(\lambda+\mathrm{i}\epsilon)\sum_i \mathbf{x}_i^2+\frac{\mathrm{i}}{2}\sum_{i<\ell}W^{\mathcal{S}}_{i\ell}(\mathbf{x}_i-\mathbf{x}_\ell)^2\right)}. \quad (15)$$

Replicated fields $\mathbf{x}_i$ are n-dimensional vector fields attached to each site i.

The Laplacian on the ring $\mathcal{R}$ is non fluctuating and we have to perform the average over the random graph $\mathcal{G}$ only. Due to the building process described in Section 2.1, the averages over different pairs of points are decoupled and we find

$$\overline{\exp\left(\frac{\mathrm{i}}{2}\sum_{i<\ell}W^{\mathcal{G}}_{i\ell}(\mathbf{x}_i-\mathbf{x}_\ell)^2\right)} = \prod_{i<\ell}\left[1-\frac{q}{N}+\frac{q}{N}\exp\left(-\frac{\mathrm{i}}{4K}(\mathbf{x}_i-\mathbf{x}_\ell)^2\right)\right] \simeq \exp\left[-\frac{qN}{2}+\frac{q}{N}\sum_{i<\ell}\exp\left(-\frac{\mathrm{i}}{4K}(\mathbf{x}_i-\mathbf{x}_\ell)^2\right)\right], \quad (16)$$

to largest order in N. An important property of the last term in (16) is that all pair of sites i, ℓ interact together with the same coupling. Therefore, introducing the density $\rho(\mathbf{x})$ of replicated vectors $\mathbf{x}_i$ equal to $\mathbf{x}$,

$$\rho(\mathbf{x}) = \frac{1}{N}\sum_{i=1}^{N}\prod_{a=1}^{n}\delta(x^a - x_i^a), \quad (17)$$

by means of a functional Lagrange multiplier $\omega(\mathbf{x})$, we obtain

$$\overline{\exp\left(\frac{\mathrm{i}}{2}\sum_{i<\ell}W^{\mathcal{G}}_{i\ell}(\mathbf{x}_i-\mathbf{x}_\ell)^2\right)} = \int\mathcal{D}\rho(\mathbf{x})\mathcal{D}\omega(\mathbf{x}) \times\exp\left[-\frac{\mathrm{i}N}{2}\int\mathrm{d}\mathbf{x}\,\omega(\mathbf{x})\rho(\mathbf{x})+\frac{\mathrm{i}}{2}\sum_{i=1}^{N}\omega(\mathbf{x}_i)-\frac{qN}{2} +\frac{qN}{2}\int\mathrm{d}\mathbf{x}\mathrm{d}\mathbf{y}\;\rho(\mathbf{x})\rho(\mathbf{y})\;\exp\left(-\frac{\mathrm{i}}{4K}(\mathbf{x}-\mathbf{y})^2\right)\right], \quad (18)$$

where the above expression includes a double path-integral over ρ and ω functions. We shall come back in Section 4.3 to the significance of the latters.

We can now take into account the contributions coming from the diagonal term and from $W^{\mathcal{R}}$ in (15). The nth moment of the partition function Z of the replicated Gaussian field theory introduced in (15)

$$\overline{Z^n} \equiv \int\prod_i \mathrm{d}\mathbf{x}_i\overline{\exp\left(\frac{\mathrm{i}}{2}(\lambda+\mathrm{i}\epsilon)\sum_i\mathbf{x}_i^2+\frac{\mathrm{i}}{2}\sum_{i<\ell}W^{\mathcal{S}}_{i\ell}(\mathbf{x}_i-\mathbf{x}_\ell)^2\right)} \quad (19)$$

may be written as

$$\overline{Z^n} = \int\mathcal{D}\rho(\mathbf{x})\mathcal{D}\omega(\mathbf{x})\;\exp\left(-N\mathcal{F}(\rho,\omega)\right), \quad (20)$$

with

$$\mathcal{F}(\rho,\omega) = \frac{\mathrm{i}}{2}\int\mathrm{d}\mathbf{x}\,\omega(\mathbf{x})\rho(\mathbf{x}) - \frac{q}{2}\int\mathrm{d}\mathbf{x}\mathrm{d}\mathbf{y}\;\rho(\mathbf{x})\rho(\mathbf{y}) \times\left[\exp\left(-\frac{\mathrm{i}}{4K}(\mathbf{x}-\mathbf{y})^2\right)-1\right] - \frac{1}{K}\log\Lambda_M(\omega). \quad (21)$$

In the above expression, $\Lambda_M(\omega)$ denotes the largest eigenvalue of a transfer matrix T we shall define in next section

and which depends on the function ω. Note that (21) is exact if N is a multiple of K.

The analogy with the theory of polymers initiated by Edwards [17,18] is clear once the ρ variables have been integrated out in (20). We are then left with a one-dimensional model of free-energy density $-\log \Lambda_M(\omega)/K$ in presence of a random potential ω distributed according to a Gaussian law. For the small-world lattice, this is no approximation since the virial expansion includes an unique corrective term to the non-interacting case, see Section 4.3.

4.2 Transfer matrix

Each element of the transfer matrix T arising in the computation of the free-energy functional (21) is labelled by $2K$ replicated vectors $\mathbf{x}_1, \mathbf{x}_2, \ldots, \mathbf{x}_K$ and $\mathbf{y}_1, \mathbf{y}_2, \ldots, \mathbf{y}_K$. From (15) and (16), T reads

$$T[\mathbf{x}_1, \mathbf{x}_2, \ldots, \mathbf{x}_K; \mathbf{y}_1, \mathbf{y}_2, \ldots, \mathbf{y}_K] = \exp\left\{ \frac{\mathrm{i}}{4}(\lambda + \mathrm{i}\epsilon) \sum_{j=1}^{K} [\mathbf{x}_j^2 + \mathbf{y}_j^2] + \frac{\mathrm{i}}{4} \sum_{j=1}^{K} [\omega(\mathbf{x}_j) + \omega(\mathbf{y}_j)] - \frac{\mathrm{i}}{8K} \sum_{1 \le j < \ell \le K} [(\mathbf{x}_j - \mathbf{x}_\ell)^2 + (\mathbf{y}_j - \mathbf{y}_\ell)^2] - \frac{\mathrm{i}}{4K} \sum_{j=1}^{K} \sum_{\ell=1}^{j} (\mathbf{x}_j - \mathbf{y}_\ell)^2 \right\}. \quad (22)$$

Due to the last term in (22), T is not a symmetric matrix. However, defining its "mirror" matrix $T^{\#}$ through

$$T^{\#}[\mathbf{x}_1, \mathbf{x}_2, \ldots, \mathbf{x}_K; \mathbf{y}_1, \mathbf{y}_2, \ldots, \mathbf{y}_K] = T[\mathbf{y}_K, \mathbf{y}_{K-1}, \ldots, \mathbf{y}_1; \mathbf{x}_1, \mathbf{x}_2, \ldots, \mathbf{x}_K], \quad (23)$$

it appears from (22) that $T = T^{\#}$. Let us now define the mirror $v^{\#}$ of a vector v through

$$v^{\#}[\mathbf{y}_1, \mathbf{y}_2, \ldots, \mathbf{y}_K] = v[\mathbf{y}_K, \mathbf{y}_{K-1}, \ldots, \mathbf{y}_1]. \quad (24)$$

Then, it can be easily checked that the left eigenvectors of T are the mirrors of its right eigenvectors. Consequently, in the large N limit, the matrix entries of T^N simplify to

$$(T^N)[\mathbf{x}_1, \mathbf{x}_2, \ldots, \mathbf{x}_K; \mathbf{y}_1, \mathbf{y}_2, \ldots, \mathbf{y}_K] \simeq (\Lambda_M)^N \, v_M^{\#}[\mathbf{y}_1, \mathbf{y}_2, \ldots, \mathbf{y}_K] v_M[\mathbf{x}_1, \mathbf{x}_2, \ldots, \mathbf{x}_K], \quad (25)$$

where v_M is the maximal eigenvector of T associated to Λ_M.

4.3 Meaning of the order parameters ρ and ω

In the large N limit, the nth moment of the partition function (19, 20) can be calculated using the saddle-point method. The optimization of the free-energy functional $\mathcal{F}$ (21) gives the values of $\rho(\mathbf{x})$ and $\omega(\mathbf{x})$, as well as $v_M[\mathbf{x}_1, \mathbf{x}_2, \ldots, \mathbf{x}_K]$ at saddle-point.

The significance of ρ is obvious from definition (17); this is the probability distribution of replicated vectors $\mathbf{x}_i$. Therefore, ρ gives access to the average resolvent (15)

$$\overline{G_{jj}^{\mathcal{S}}(\lambda + \mathrm{i}\epsilon)} = \lim_{n \to 0} -\frac{\mathrm{i}}{n} \int \mathrm{d}\mathbf{x} \, \rho(\mathbf{x}) \, \mathbf{x}^2, \quad (26)$$

and to the density of states through (2).

More generally, within the transfer matrix formalism developed in Section 4.2, the joint probability distribution of replicated vectors $\mathbf{x}_i, \mathbf{x}_{i+1}, \ldots, \mathbf{x}_{i+K-1}$ is related to the maximal eigenvector v_M of T. Normalizing v_M to unity, this joint probability reads (25)

$$\rho_{\mathrm{joint}}(\mathbf{x}_i, \mathbf{x}_{i+1}, \ldots, \mathbf{x}_{i+K-1}) = v_M[\mathbf{x}_i, \mathbf{x}_{i+1}, \ldots, \mathbf{x}_{i+K-1}] \, v_M^{\#}[\mathbf{x}_i, \mathbf{x}_{i+1}, \ldots, \mathbf{x}_{i+K-1}]. \quad (27)$$

In particular, the one point density ρ is found back when all but one vectors are integrated out in the above formula

$$\rho(\mathbf{x}) = \int \mathrm{d}\mathbf{x}_2 \ldots \mathrm{d}\mathbf{x}_K \, v_M[\mathbf{x}, \mathbf{x}_2, \ldots, \mathbf{x}_K] \, v_M^{\#}[\mathbf{x}, \mathbf{x}_2, \ldots, \mathbf{x}_K]. \quad (28)$$

Identity (28) is precisely the stationary condition of $\mathcal{F}$ (21) with respect to ω.

The meaning of ω is less straightforward but emerges from the extremization condition of $\mathcal{F}$ with respect to ρ,

$$\frac{\mathrm{i}}{2}\omega(\mathbf{x}) = q \int \mathrm{d}\mathbf{y} \, \rho(\mathbf{y}) \left[\exp\left(-\frac{\mathrm{i}}{4K} (\mathbf{x} - \mathbf{y})^2 \right) - 1 \right]. \quad (29)$$

The above equation is strongly reminiscent of the first correction to the logarithm of the density obtained from Mayer's expansion of interacting gas [33]. Indeed, this close relationship has been exposed in [27] (see also [34] for the similar case of finite-connectivity spin-glasses). The replicated field $\mathbf{x}_i$ attached to site i may be interpreted as the position of particle i in a $n-$dimensional abstract space. Particles see an external harmonic potential $-\frac{\mathrm{i}}{2}(\lambda + \mathrm{i}\epsilon)\mathbf{x}^2$ and interact with each other through a two-body quadratic energy $-\frac{\mathrm{i}}{2} W_{ij}^{\mathcal{S}} (\mathbf{x}_i - \mathbf{x}_j)^2$, see (19). In the absence of any $W^{\mathcal{S}}$ matrix, the density of a non-interacting gas is recovered

$$\rho_0(\mathbf{x}) = \exp\left(\frac{\mathrm{i}}{2}(\lambda + \mathrm{i}\epsilon)\mathbf{x}^2 \right), \quad (30)$$

obtained from equation (19). The first virial coefficient, that is the first correction to $\log \rho(\mathbf{x})$ in the expansion in powers of ρ (and not in powers of the fugacity ρ_0) is precisely given by the r.h.s of (29) [27,33]. It turns out that Mayer's expansion for random graph do not include higher order terms, as is expected from the similarity between random graph and trees.

Therefore, $-\frac{\mathrm{i}}{2}\omega(\mathbf{x})$ may be understood as the effective potential due to interactions with other particles seen by a particle located in $\mathbf{x}$. This interpretation will be useful in deriving the single defect approximation of Section 6.

4.4 Autocorrelation function of the eigenvectors

We have seen in Section 2.2 that the autocorrelation functions of eigenvectors are related to the resolvent $\overline{G^{\mathcal{S}}_{jk}}$, see identity (4). By definition, the latter is the average scalar product of replicated vectors $\mathbf{x}_j$ and $\mathbf{x}_k$ (15) with the Gaussian measure (19). Within the transfer matrix formalism we have introduced in Sections 4.2 and 4.3, this mean dot product can be computed from the knowledge of all eigenvectors v_ℓ and eigenvalues Λ_ℓ of T. We decompose the distance $d = |j-k|$ between sites j and k as $d = d_0 + K\, d_1$ with $0 \leq d_0 \leq K-1$ and d_1 integer-valued. Then the average resolvent reads

$$\overline{G^{\mathcal{S}}_{jk}(\lambda+\mathrm{i}\epsilon)} = \lim_{n\to 0} -\mathrm{i}\sum_{\ell=1}^{\infty} \langle v_M^{\#}\cdot X_1^1 \cdot v_\ell\rangle \langle v_\ell^{\#}\cdot X^1_{1+d_0}\cdot v_M\rangle \left(\frac{\Lambda_\ell}{\Lambda_M}\right)^{d_1}. \tag{31}$$

In the above equation, the maximal eigenvalue of T coincides with $\ell = 1$ ($\Lambda_1 \equiv \Lambda_M$) and increasingly excited states correspond to $\ell \geq 2$. The X_b^a operator measures the value of the ath component of the replicated field $\mathbf{x}$ appearing at the bth place in v_ℓ (with $1 \leq b \leq K-1$) and $\langle v_M^{\#}\cdot X\cdot v_\ell\rangle$ denotes the matrix element of X_b^a between states v_M and v_ℓ,

$$\langle v_M^{\#}\cdot X_b^a \cdot v_\ell\rangle = \int \mathrm{d}\mathbf{x}_1 \ldots \mathrm{d}\mathbf{x}_K\; x_b^a\; v_M^{\#}[\mathbf{x}_1,\mathbf{x}_2,\ldots,\mathbf{x}_K]\; v_\ell[\mathbf{x}_1,\mathbf{x}_2,\ldots,\mathbf{x}_K]. \tag{32}$$

For small distances $\mathrm{d} \leq K-1$, $d_1 = 0$ and the sum over eigenstates in formula (31) can be carried out to obtain

$$\overline{G^{\mathcal{S}}_{jk}(\lambda+\mathrm{i}\epsilon)} = \lim_{n\to 0} -\mathrm{i}\langle v_M^{\#}\cdot X_1^1\; X^1_{1+d}\cdot v_M\rangle,\; 0 \leq d \leq K-1. \tag{33}$$

Using identity (28), the above equation gives back the $d = 0$ resolvent (26).

Expression (31) may also be used to compute the autocorrelation function of eigenvectors at large distance d, that is when the sum in (31) is dominated by the $\ell = 2$ contribution. The ratio $\tau = \Lambda_2/\Lambda_M$ whose modulus is by definition smaller than (or equal to) unity can be written as

$$\tau = \exp\left(-K\sigma + \mathrm{i}2\pi K\phi\right), \tag{34}$$

with $\sigma \geq 0$. Therefore, at large distances d, the average resolvent scales as

$$\overline{G^{\mathcal{S}}_{jk}(\lambda+\mathrm{i}\epsilon)} \sim \exp(-\sigma d + \mathrm{i}2\pi\phi d), \tag{35}$$

where both σ and ϕ depend on the energy level λ. Consequently, σ may be seen as the inverse autocorrelation length of the eigenmodes associated to level λ and ϕ as the typical wave number of the latters. We shall explicitly compute the inverse length σ and wave number ϕ in Section 5.4 within the effective medium approximation and compare them to the numerical results of Section 3.2.

5 Effective medium approximation

The exact extremization of free-energy function (21) is an awkward task. We start by solving this problem using an effective medium approximation (EMA) which gives a good description of the extended part of the spectrum.

5.1 Presentation of the approximation

The starting point of EMA is the exact expression of the density ρ obtained from (19) [27],

$$\rho(\mathbf{x}) = \frac{1}{N}\overline{\sum_{i=1}^{N} C_i \exp\left(\frac{\mathrm{i}\,\mathbf{x}^2}{2[(\lambda+\mathrm{i}\epsilon)1 - W^{\mathcal{S}}]^{-1}_{ii}}\right)}, \tag{36}$$

where the C_i are normalization constants going to unity as n vanishes.

In the extended part of the spectrum, we expect all matrix elements appearing in (36) to be of the same order of magnitude and thus $\rho(\mathbf{x})$ to be roughly Gaussian. We therefore assume the following Ansatz for the density

$$\rho^{\mathrm{EMA}}(\mathbf{x}) = \left(2\pi\mathrm{i}g^{\mathrm{EMA}}\right)^{-\frac{n}{2}} \exp\left(\frac{\mathrm{i}\,\mathbf{x}^2}{2\,g^{\mathrm{EMA}}}\right). \tag{37}$$

In addition, the effective potential ω we choose to be harmonic, see Section 4.3,

$$\omega^{\mathrm{EMA}}(\mathbf{x}) = \hat{g}^{\mathrm{EMA}}\,\mathbf{x}^2. \tag{38}$$

EMA is therefore implemented by inserting the Gaussian Ansatz (37, 38) into functional $\mathcal{F}$. Due to the choice (38) for ω, the transfer matrix T simplifies to the tensorial product of n identical matrices

$$T^{\mathrm{EMA}}[x_1,x_2,\ldots,x_K;y_1,y_2,\ldots,y_K] = \exp\left\{\frac{\mathrm{i}}{4}(\hat{g}^{\mathrm{EMA}}+\lambda+\mathrm{i}\epsilon)\sum_{j=1}^{K}[x_j^2+y_j^2] - \frac{\mathrm{i}}{8K}\sum_{1\leq j<\ell\leq K}[(x_j-x_\ell)^2+(y_j-y_\ell)^2] - \frac{\mathrm{i}}{4K}\sum_{j=1}^{K}\sum_{\ell=1}^{j}(x_j-y_\ell)^2\right\}. \tag{39}$$

The resulting free-energy per replica reads in the limit $n \to 0$,

$$\mathcal{F}^{\mathrm{EMA}}(g^{\mathrm{EMA}},\hat{g}^{\mathrm{EMA}}) = -\frac{1}{2}g^{\mathrm{EMA}}\hat{g}^{\mathrm{EMA}} + \frac{q}{4}\log\left(1-\frac{g^{\mathrm{EMA}}}{K}\right) - \frac{1}{K}\log\Lambda_M^{\mathrm{EMA}}(\hat{g}^{\mathrm{EMA}}), \tag{40}$$

where $\Lambda_M^{\mathrm{EMA}}(\hat{g}^{\mathrm{EMA}})$ is the largest eigenvalue of T^{EMA} (39).

5.2 Self-consistent equations

To compute $\Lambda_M^{\rm EMA}(\hat{g}^{\rm EMA})$, we take advantage of the Gaussian structure of $T^{\rm EMA}$ and look for a maximal eigenvector of the form

$$v_M^{\rm EMA}[x_1, x_2, \ldots, x_K] = v_0 \exp\left(\frac{\rm i}{2}\sum_{q,r=1}^{K} V_{qr}\ x_q\ x_r\right), \tag{41}$$

where v_0 is a normalization constant. The self-consistent equations fulfilled by the $K\times K$ matrix V are immediately obtained and read

$$\begin{aligned} V_{qr} &= \frac{1}{2}\delta_{qr}\left(\hat{g}^{\rm EMA}+\lambda+{\rm i}\epsilon-\frac{q}{K}-\frac{1}{2}\right)+\frac{1}{4K} \\ &\quad -\frac{1}{4K^2}\sum_{s=1}^{q}\sum_{t=1}^{r}\left(U^{-1}\right)_{st} \\ U_{qr} &= V_{qr}+\frac{1}{2}\delta_{qr}\left(\hat{g}^{\rm EMA}+\lambda+{\rm i}\epsilon-\frac{K+1-q}{K}-\frac{1}{2}\right)+\frac{1}{4K}, \end{aligned} \tag{42}$$

where δ denotes the Kronecker symbol. The saddle-point equations of $\mathcal{F}^{\rm EMA}$ with respect to $g^{\rm EMA}$ and $\hat{g}^{\rm EMA}$ respectively read

$$\hat{g}^{\rm EMA} = \frac{q}{2(g^{\rm EMA}-K)} \tag{43}$$

$$g^{\rm EMA} = \frac{1}{K}\ {\rm Tr}\left[\left(V+V^{\#}\right)^{-1}\right]. \tag{44}$$

The saddle-point equation (28) gives back equation (44) while identity (43) differs from (29) since the EMA order parameters (37, 38) are not exact solutions of the extremization conditions over $\mathcal{F}$.

We have solved numerically the above self-consistency equations using the following procedure. For given K, q and λ, we start with an arbitrary value of $g^{\rm EMA}$, *e.g.* null, and compute $\hat{g}^{\rm EMA}$ from (43). We then seek for matrices V and U fulfilling (42). Among all possible solutions, we select the matrix V having all eigenvalues with positive imaginary parts so that $v_M^{\rm EMA}$ (41) is bounded for large arguments $\mathbf{x}$. The new value of $g^{\rm EMA}$ is computed from (44). The whole process is iterated until a fixed value of $g^{\rm EMA}$ has been found. The density of states is then equal to the imaginary part of $g^{\rm EMA}$ divided by $-\pi$, see in order (37), (26) and (2).

5.3 Spectrum, mobility edge and pseudo-gap

The density of states obtained for $K=3$, $q=1$ and $q=5$ are shown Figures 2a and 3a respectively. The overall form of the EMA spectrum coincides with the numerics. The quantitative agreement is of course less precise at large disorder ($q=5$). We shall see in Section 6.3 how the theoretical spectrum may be improved using SDA.

On the right side of the spectrum, the mobility edge is accurately estimated: $\lambda_+^{\rm EMA}\simeq 2.13$ for $q=1$ and $\lambda_+^{\rm EMA}\simeq 3.35$ for $q=5$, compare to Section 3.1. Nevertheless, as expected from the presentation of EMA in Section 5.1, the oscillations of $p(\lambda)$ corresponding to non-extended states are not captured by the approximation.

A similar situation takes place at small energy levels. EMA predicts a gap whose order of magnitude ($\lambda_-^{\rm EMA}\simeq 0.064$ for $q=1$ and $\lambda_-^{\rm EMA}\simeq 0.46$ for $q=5$) coincides with the findings of Section 3.1. However, from a qualitative point of view, EMA wrongly predicts a vanishing density of state below $\lambda_-^{\rm EMA}$. This artifact is well known in the case of the Bethe lattice [10,12,30] for which EMA becomes exact.

We have analytically checked the scaling behaviour discussed in Section 2.5 in the simplest case $K=1$. In the small q,λ region the EMA resolvent is obtained from Section 5.2,

$$g^{\rm EMA}\simeq\frac{-q+\sqrt{q^2-8\lambda}}{4\lambda}\,. \tag{45}$$

The gap width is therefore given by $\lambda_-^{\rm EMA}\simeq q^2/8$, in agreement with the heuristic arguments of Section 2.5 indicating that the size of the pseudo-gap scales as $O(q^2)$ for weak disorder. Furthermore, the cross-over between "one-dimensional" behaviour and rare events take place when the imaginary part of the resolvent (45) reaches its maximum, that is at $\lambda_{\rm c.o.}\simeq q^2/4$. The corresponding density of states scales as $p_{\rm c.o.}\simeq 1/q$, in quantitative agreement with the findings of Section 2.5. Notice also that the value of the ratio $\lambda_{\rm c.o.}/\lambda_-\simeq 2$ is supported by the numerical results for $K=3$, see Section 3.1.

5.4 Relations of dispersion

We have shown in Section 4.4 that the autocorrelation function of eigenvectors is accessible from the second largest eigenvalue Λ_2 of T (22). Due to the similarity of $T^{\rm EMA}$ (39) with the evolution operator of a quantum oscillator, we look for an eigenvector of the following form

$$v_2^{\rm EMA}[x_1, x_2, \ldots, x_K] = v_1 \exp\left(\frac{\rm i}{2}\sum_{q,r=1}^{K} V_{qr}\ x_q\ x_r\right)\ \sum_{r=1}^{K}\gamma_r x_r, \tag{46}$$

where v_1 is a normalization constant and V_{qr} is the quadratic form appearing in the maximal eigenvector v_M and self-consistently defined through (42). An elementary calculation shows that the above Ansatz indeed corresponds to an eigenvector of $T^{\rm EMA}$ if and only if the K coefficients γ_r arising in (46) fulfill the eigensystem

$$\tau\ \gamma_r = -\frac{1}{2K}\sum_{q=r}^{K}\sum_{s=1}^{K}(U^{-1})_{qs}\ \gamma_s, \tag{47}$$

where U has been defined in (42) and $\tau=\Lambda_2/\Lambda_M$. We are thus left with the diagonalization of a $K\times K$ matrix

whose complex eigenvalues $\tau_\ell, \ell = 1, \ldots, K$ can be written as (34),

$$\tau_\ell = \exp\left(-K\sigma_\ell + \mathrm{i}2\pi K\phi_\ell\right). \tag{48}$$

In doing so, we have at our disposal the first K excited states of T and not only the first one. This is a peculiarity of the EMA scheme, that was not expected from Section 4.4. The average resolvent therefore obeys the asymptotic scaling (35)

$$\overline{G^{\mathcal{S}}_{jk}(\lambda + \mathrm{i}\epsilon)} \sim \sum_{\ell=1}^{K} C_\ell \ \exp(-\sigma_\ell d + \mathrm{i}2\pi\phi_\ell d). \tag{49}$$

This large distance behaviour strengthens the data modelling (14) used in Section 3.3. Indeed, if relation (49) held for all d's, the power spectrum of the eigenvectors $|\tilde{w}(\theta,\lambda)|^2$ would be well approximated by a superposition of Lorentzian factors from equation (4).

The wave numbers ϕ_ℓ as well as the inverse autocorrelation lengths σ_ℓ are plotted Figures 6 and 7 *vs.* the eigenvalue λ for $K = 3, q = 1$ and $K = 3, q = 5$ respectively. The agreement between the EMA prediction and the numerical results of Section 3.2 is good. Notice that numerical points for the wave numbers ϕ_1 and ϕ_2 merge and lie between the theoretical branches when λ approaches λ_+. This phenomenon is simply due to the coalescence of the first two peaks in (14) when $|\phi_2 - \phi_1| \simeq \sigma_1/2\pi$ arising at such energy levels.

In the extended part of the spectrum, EMA can therefore be used to obtain some accurate effective relations of dispersion for the eigenmodes of the Laplacian operator, even at strong disorder.

6 Single defect approximation

6.1 Principle of the approximation

The physical grounds of the single defect approximation have been exposed in [27]. The basic idea is to treat exactly, *via* the stationarity equations (28, 29) the interactions of a single site, *i.e.* the defect with its surrounding neighbors belonging to the effective medium [30] *taking into account the fluctuations of the number of these neighbors* [27]. This approximation scheme amounts to perform one iteration of the extremization condition on the free-energy functional $\mathcal{F}$ from the EMA solution. Let us see how SDA works for the small-world problem.

First, we consider the saddle-point equation for the effective potential (29). When inserting the EMA density (37) in the r.h.s. of (29), we obtain the SDA effective potential

$$\frac{\mathrm{i}}{2}\,\omega^{\mathrm{SDA}}(\mathbf{x}) = q\,\left[\exp\left(\frac{\mathrm{i}\,\mathbf{x}^2}{2(g^{\mathrm{EMA}} - 2K)}\right) - 1\right], \tag{50}$$

up to irrelevant terms when $n \to 0$. This expression differs from the best quadratic potential obtained from EMA (38, 43).

To calculate the SDA density ρ^{SDA}, the stationarity identity (28) requires the eigenvector of the transfer matrix (22) in presence of the SDA potential (50). Such a calculation cannot be done analytically. Remembering the interpretation of ω exposed in Section 4.4, we may however estimate the ratio of the probabilities that a particle be located in the n-dimensional abstract space at position $\mathbf{x}$ within each scheme of approximation by

$$\begin{aligned}\frac{\rho^{\mathrm{SDA}}(\mathbf{x})}{\rho^{\mathrm{EMA}}(\mathbf{x})} &\simeq \exp\left[\frac{\mathrm{i}}{2}\,\omega^{\mathrm{SDA}}(\mathbf{x}) - \frac{\mathrm{i}}{2}\,\omega^{\mathrm{EMA}}(\mathbf{x})\right] \\ &\simeq \sum_{c=0}^{\infty} \frac{\mathrm{e}^{-q}\,q^c}{c!} \exp\left[\frac{\mathrm{i}}{2}\left(\frac{c}{g^{\mathrm{EMA}} - 2K} - \hat{g}^{\mathrm{EMA}}\right)\mathbf{x}^2\right].\end{aligned} \tag{51}$$

As in the simpler case of the random graph [27], the anharmonicity of the effective potential ω^{SDA} (50) reflects the local fluctuations of connectivity. Using the above expression for ρ^{SDA}, we can now study the localized states induced by the geometrical defects we have observed in Section 3.3.

6.2 Localized eigenvalues

The second moment of the field $\mathbf{x}$ in the SDA scheme reads, see (26, 37, 51),

$$\begin{aligned} g^{\mathrm{SDA}} &= \lim_{n\to 0} -\frac{\mathrm{i}}{n}\int \mathrm{d}\mathbf{x}\,\rho^{\mathrm{SDA}}(\mathbf{x})\,\mathbf{x}^2, \\ &= \sum_{c=0}^{\infty} \frac{\mathrm{e}^{-q}\,q^c}{c!}\left(\frac{1}{g^{\mathrm{EMA}}} + \frac{c}{g^{\mathrm{EMA}} - 2K} - \hat{g}^{\mathrm{EMA}}\right)^{-1}. \end{aligned} \tag{52}$$

Above the mobility edge λ_+^{EMA}, the EMA density of states vanishes. Thus, $g^{\mathrm{EMA}}(\lambda)$ and $g^{\mathrm{SDA}}(\lambda)$ are real numbers. However, the poles of g^{SDA} located on the real axis can give rise to Dirac peaks in the density of states [27]. Consider indeed such a singularity taking place at $\lambda_{\mathrm{sing}} > \lambda_+^{\mathrm{EMA}}$. Close to the singularity, we may write

$$g^{\mathrm{SDA}}(\lambda) \sim \frac{p_{\mathrm{sing}}}{\lambda - \lambda_{\mathrm{sing}} + \mathrm{i}\epsilon}, \tag{53}$$

and obtain a contribution to the density of states equal to $p_{\mathrm{sing}}\,\delta(\lambda - \lambda_{\mathrm{sing}})$ using (2). As seen from expression (52), the poles of g^{SDA} form a discrete sequence of energy levels λ_c^{SDA} labelled by the integer number c. The values of λ_c^{SDA} and of the corresponding weights p_c^{SDA} are listed Table 1 and Table 2 for $K = 3, q = 1$ and $K = 3, q = 5$ respectively. The agreement with the numerical values of Section 3.1 is good (see that section for a discussion of the reliability of numerical measures). Note that c coincides with the coordination number of the centers of eigenmodes measured in Section 3.3. This strongly supports the statement that defects are responsible for localization [27].

6.3 Extended spectrum at strong disorder

The EMA density of states for $K = 3, q = 5$ displayed Figure 3a shows some discrepancies with the numerics from the maximum density located at $\lambda \simeq 1.5 - 2.0$ up to the mobility edge. We have computed the SDA density of

states in the extended region from equations (52) and (2). The result is shown Figure 3a and agrees in a much better way with numerics.

For completeness, we have also compute the SDA density of states at low disorder $K = 3, q = 1$ in the extended region. The resulting spectrum can hardly be distinguished from the EMA prediction, and is therefore in very good agreement with numerics.

7 Summary and conclusion

In this work, the spectral properties of the Laplacian operator on mixed lattices, composed of a random graph structure superimposed to a unidimensional ring have been investigated. Using some approximation schemes, we have been able to reproduce the numerical density of states with a good agreement and to obtain a quantitative description of the localized eigenstates. From this point of view, we have shown that the single defect approximation introduced in the simpler context of the random graph was also capable of giving reliable and precise estimates of the localized energies in presence of a finite-dimensional underlying geometry.

One of the most interesting aspects of the present work is the existence of pseudo dispersion relations for disordered and thus non periodic lattices. By studying the autocorrelation functions of eigenmodes, or more precisely their power spectra we have shown that some features of the pure lattice remain present even at strong disorder. It is encouraging to notice that the effective medium approximation already provides a very good description of the power spectra of the eigenmodes. To what extent this result holds in higher dimensional models is of course questionable.

As emphasized in the introduction, the small-world architecture may be of particular relevance to the field of polymers and more generally chain-like systems with three-dimensional interactions, *e.g.* proteins, DNA, ... With respect to the diffusion problem studied here, realistic models of polymers or biological molecules have to take into account the internal degrees of freedom of the monomers/constituents and their non-trivial interactions. We hope nevertheless that the technical approach developed in the present paper will be of use in these more complex cases. In particular, the knowledge of the excited states of the self-consistent transfer matrix should give access to the effective dispersion relations of the eigenmodes. The latters are of primary importance to understand the dynamical properties of such molecules [35,36], with possible applications to the relaxation of single DNA molecules [37].

I am particularly grateful to G. Biroli for numerous comments and suggestions about this work. I also thank A. Barrat, S. Cocco, M. Weigt and R. Zecchina for useful discussions.

References

1. A. Ishimaru, *Wave propagation in random media* (Academic Press, New-York, 1978).
2. B. Souillard, *Waves and electrons in random media, Chance and Matter, Les Houches session XLVI* (Elsevier Science, 1986).
3. J.P. Wolfe, *Imaging phonons, acoustic wave propagation in solids* (Cambrigde University Press, Cambridge, 1998).
4. S. Havlin, D. Ben Avraham, Adv. Phys. **36**, 695 (1987).
5. J.P. Bouchaud, A. Georges, Phys. Rep. **195**, 217 (1990).
6. P.W. Anderson, Phys. Rev. **109**, 1492 (1958).
7. D.J. Thouless, Phys. Rep. **13**, 93 (1974); *Mesoscopic quantum physics, Les Houches session LXI* (Elsevier Science, 1995).
8. S.R. Elliott, *Physics of Amorphous Materials* (Longman Scientific and Technical, London, 1990).
9. E. Abrahams, P.W. Anderson, D.C. Licciardello, T.V. Ramakrishnan, Phys. Rev. Lett. **42**, 673 (1979).
10. R. Abou-Chacra, P.W. Anderson, D.J. Thouless, J. Phys. C **6**, 1734 (1973).
11. I.A. Campbell, J. Phys. Lett. France **46**, L1159 (1985).
12. A.J. Bray, G.J. Rodgers, Phys. Rev. B **38**, 11461 (1988).
13. D.J. Watts, S.H. Strogatz, Nature **393**, 440 (1998).
14. M. Barthelemy, L.A. Nunes Amaral, Phys. Rev. Lett. **82**, 3180 (1999); A. Barrat, comment on *Small-world networks: evidence for a cross-over picture*, `cond-mat/9903323` (1999).
15. A. Barrat, M. Weigt, *On the properties of small-world network models*, `cond-mat/9903411` (1999).
16. M.E.J. Newman, D.J. Watts, *Renormalization group analysis of the small-world network model*, Santa Fe Institute working paper 99-04-029, `cond-mat/9903357` (1999); M.E.J. Newman, D.J. Watts, *Scaling and percolation in the small-world network model*, Santa Fe Institute working paper 99-05-034, `cond-mat/9904419` (1999).
17. P.G. de Gennes, *Scaling concepts in polymer physics* (Cornell University Press, 1979).
18. S.F. Edwards, Proc. Phys. Soc. London **85**, 613 (1965).
19. P.G. de Gennes, Rep. Prog. Phys. **32**, 187 (1969).
20. B.H. Zimm, J. Chem. Phys. **24**, 269 (1956).
21. L. Harnau, R.G. Winkler, P. Reineker, J. Chem. Phys. **104**, 6355 (1996).
22. T. Keyes, J. Phys. Chem. A **101**, 2921 (1997).
23. T.-M. Wung, R.F. Loring, J. Chem. Phys. **97**, 8568 (1992).
24. Y. Wan, R. Stratt, J. Chem. Phys. **100**, 5123 (1994).
25. G.J. Rodgers, C. De Dominicis, J. Phys. A **23**, 1567 (1990).
26. Y.V. Fyodorov, A.D. Mirlin, J. Phys. A **24**, 2219 (1991).
27. G. Biroli, R. Monasson, J. Phys. A **32**, L255 (1999).
28. J. Bellissard, D.S. Dean, *Spectral Properties of the Laplacian on Random Graphs*, preprint (1999).
29. A. Cavagna, I. Giardina, G. Parisi, *Analytic computation of the Instantaneous Normal Modes spectrum in low density liquids*, `cond-mat/9903155` (1999).
30. R. Kulas, M.F. Thorpe, *A model for phonons in compound amorphous materials*, in *Structure and Excitations of Amorphous Solids*, edited by G. Lucovsky, F.L. Galeener (AIP Conference Proceedings, New-York, 1976).
31. L.A. Pastur, *Introduction to the theory of disordered systems* (Wiley Interscience Publications, New-York, 1988).
32. D. Sornette, J. Stat. Phys. **56**, 669 (1989).
33. T. Morita, K. Hiroike, Prog. Theor. Phys. **25**, 537 (1961).
34. R. Monasson, J. Phys. A **31**, 513 (1998).
35. G. Gaeta, C. Reiss, M. Peyrard, T. Dauxois, Nuovo Cim. **17**, 1 (1994) and references therein.
36. S. Cocco, M. Barbi, M. Peyrard, Phys. Lett. A **253**, 358 (1999).
37. L. Harnau, P. Reineker, New Journal of Physics **1**, 3.1 (1999). (`http://www.njp.org/`) and references about experiments therein.